Understanding Adsorption of Violanthrone-79 as a Model Asphaltene Compound on Quartz Surface Using Molecular Dynamics Simulations

Tu Lan,[†,‡] Hongbo Zeng,[*,†] and Tian Tang,[*,‡]

[†]Department of Chemical and Materials Engineering, University of Alberta, Edmonton, AB T6G 1H9, Canada

[‡]Department of Mechanical Engineering, University of Alberta, Edmonton, AB T6G 1H9, Canada

ABSTRACT: A series of molecular dynamics simulations were performed to investigate the adsorption of violanthrone-79 (VO-79) as a model asphaltene compound on quartz surface in different organic solvents (*n*-heptane, toluene and heptol with 3 different *n*-heptane/toluene volume ratios). Our simulations demonstrated that the type of solvent had a great impact on the kinetics of adsorption, such as the adsorption rate and final adsorption amount. However, the equilibrium modes of adsorption were similar: both monomer and aggregate adsorptions were observed regardless of the *n*-heptane and toluene content. With monomer adsorption, the polyaromatic core (PAC) of VO-79 was merely parallel to the surface; while the PACs showed two types of orientations in aggregate adsorption: parallel and slant, with the majority of them slant to the surface maintaining π-π stacking between neighboring PACs. Energetic analyses showed that the adsorption was driven primarily by van der Waals forces, accompanied by electrostatic interactions, hydrogen bonding and free energy of solvation. The results reported here provide valuable insights at the molecular level into the mechanistic understanding of asphaltenes adsorption on mineral surfaces in organic media.

1. INTRODUCTION

Adsorption of asphaltenes on mineral surfaces is a ubiquitous, undesirable phenomenon in oil production.[1] It can modify the wettability of mineral surfaces from water-wet to oil-wet, rendering the surfaces hydrophobic, causing reservoir damage as well as corrosion and fouling in downstream operations.[2-5] Understanding the adsorption of asphaltenes on mineral surfaces is therefore important in order to propose methods to prevent, minimize or reverse the adsorption.

Over the past decade, many studies have examined asphaltene adsorption on minerals.[6-23] Several studies suggested that in toluene and heptol (mixture of *n*-heptane and toluene) solutions asphaltenes or their aggregates did not penetrate into the interlayers of clays and were adsorbed only on their surfaces.[6, 7] Both monolayer and multilayer adsorption have been observed in experiments.[21-24] For example, Dudášová et al.[23] investigated the adsorption of asphaltenes from five different origins onto minerals and clays (kaolin, $CaCO_3$, $BaSO_4$, FeS, Fe_3O_4, TiO_2 and SiO_2) in heptol , and found that the Langmuir isotherm model fitted well to all of the experimental isotherms. Their results indicated that the adsorption of asphaltenes was in the form of a monolayer, and the adsorption capacities were determined to vary from 0.26 to 3.78 mg/m^2. Multilayer adsorption generally occurred at high asphaltene concentration[21] or in solvents where asphaltenes had poor solubility such as *n*-heptane and dodecane.[22] The adsorption was attributed to different forces, including electrostatics, charge-transfer, van der Waals, and hydrogen bonding.[19-21, 25] The effects of many factors on asphaltene adsorption have also been investigated, such as temperature, pressure, salinity, asphaltene concentration, and the type of solvent.[9-13, 21]

Molecular dynamics (MD) simulations, which can provide insights into dynamic processes at molecular level, have been widely employed to investigate the behaviors of heavy oil compounds, such as asphaltenes, in bulk solution and on oil/water interfaces,[26-35] with only a few recent studies tackling their adsorption on mineral surfaces.[36-38] Real asphaltenes are a complex mixture of polyaromatic compounds and depending on the source of the crude oil, there can be large variations in their composition. Because of this, past MD simulations all employed certain type(s) of model compounds that represented some features of asphaltenes. The most commonly considered asphaltene model compounds include violanthrone-78 (VO-78), violanthrone-79 (VO-79) and *N*-(1-hexylheptyl)-*N'*-(5-carboxylicpentyl)-perylene-3,4,9, 10-tetracarboxylic bisimide (C5Pe).[32-35, 37-43] They are similar, in structure, to the

island-type asphaltenes proposed in the literature,[44] and have been successfully used to mimic asphaltenes in crude oil.[31-35, 37-41] Wu et al.[36] used model compounds to represent asphaltene, resin, aromatic and saturate fractions of heavy crude oil, and investigated their sorption, diffusion and distribution on quartz surface. Insignificant difference was found in the diffusivities of asphaltene, resin and aromatic on the surface, which indicated that van der Waals interaction was the main contributor to the sorption of these components. Recently, the adsorption of C5Pe on silica from *n*-heptane and toluene was simulated using MD.[37] Van der Waals force was again shown to provide the largest contribution to adsorption, although hydrogen bonds were found to form between the polar terminal group (carboxylic acid) of C5Pe and the silanol groups of silica. Compared with toluene, C5Pe showed less self-aggregation in bulk heptane and more adsorption on silica. The same authors also studied the simultaneous adsorption of C5Pe and *N*-(1-undecyldodecyl)-*N*′-(5-carboxylicpentyl)-perylene-3,4,9,10 -tetracarboxylic bisimide (C5PeC11) on silica, with heptol (equal volume of *n*-heptane and toluene) being the solvent.[38] A clear synergy between C5Pe and C5PeC11 was demonstrated, which enhanced their adsorption through π–π stacking and T-stacking between polyaromatic cores, as well as hydrogen bonding between their polar terminal groups and silica.

Variation in chemical structure of the model compounds is known to influence their behaviors in bulk solvents and on interfaces.[45-47] For instance, when the polar terminal of C5Pe was substituted by an aliphatic functional group, the molecules did not form polyaromatic π–π stacking in bulk *n*-heptane or toluene.[45] Given that the polar terminal groups in C5Pe contribute significantly to adsorption, and that real asphaltene may contain molecules with different degrees of polarity,[48-50] it is of interest to investigate what would happen to asphaltene adsorption on mineral surfaces in absence of these polar terminal groups. Motivated by this, in this work we chose a different model compound, namely VO-79, which contains nine fused aromatic rings attached with two aliphatic side chains. Using MD simulations, we study the adsorption of VO-79 on quartz surface in different organic solvents (*n*-heptane, toluene, and heptol with three *n*-heptane/toluene volume ratios). The objective is to provide a molecular level understanding on the dynamics, structure and mechanisms of the adsorption and address the effect of solvents with different solubility.

2. SIMULATION METHODS

2.1 Models and Systems Simulated. VO-79 ($C_{50}H_{48}O_4$), shown in Figure 1a, was chosen as the model asphaltene, which has a central polyaromatic core (PAC) and two side chains (SCs). Most silicas employed in adsorption studies are microporous containing many hydroxyl groups on the surface,[51] and the hydroxylated silica surfaces are known to enable the adsorption of organic and biologic molecules.[52, 53] Based on this, a hydroxylated quartz surface was used in this work to mimic the mineral surface. To reduce the complexity of the model while maintaining the key functional groups for adsorption, a monolayer quartz surface was created with the silanol (Si−OH) groups on one side of the surface and Si−H groups on the other (Figure 1b). The force field parameters for quartz and the partial atomic charges of silanol groups were adopted from existing literatures,[54-56] which have been validated and used to investigate the interaction between oil and silica.[37, 57-59] The organic solvents were represented by *n*-heptane, toluene and heptol. The topologies for VO-79, *n*-heptane and toluene were created and validated in our previous work,[35, 60-62] and directly adopted here.

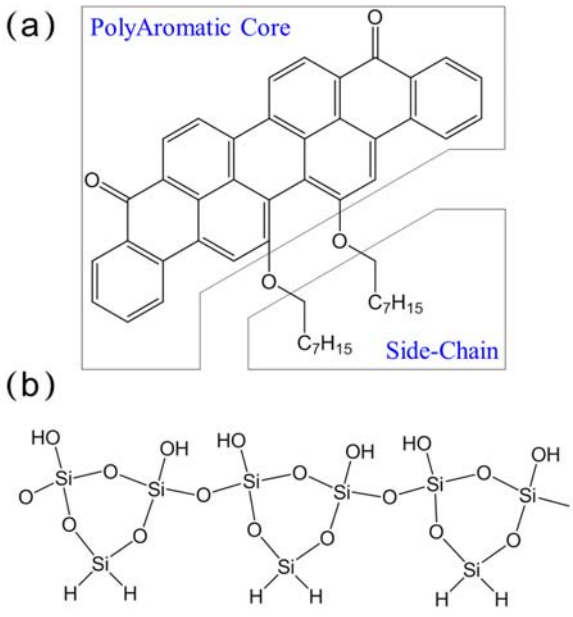

Figure 1. Molecular structure of (*a*) violanthrone-79 as a model asphaltene and (*b*) hydroxylated quartz surface employed in this work.

To systematically probe the adsorption of VO-79 on quartz surface under the influence of different solvents, 5 systems were constructed. Details of these systems are summarized in Table 1. For each system, a simulation box of 5.7 × 5.6 × 11 nm^3 was

first built which contained 24 VO-79 molecules. The 24 molecules were arranged with their PACs parallel to one another, forming a 4 × 2 × 3 array. The rest of the box was filled with a particular type of organic solvents: pure *n*-heptane in system H100, heptol with 25% toluene and 75% *n*-heptane in system HT25, heptol with 50% toluene and 50% *n*-heptane in system HT50, heptol with 75% toluene and 25% *n*-heptane in system HT75, and pure toluene in system T100. After an initial steepest descent energy minimization to ensure that the maximum force is less than 1000.0 kJ/(mol × nm), the system was equilibrated at 300 K within position restraint on the VO-79 molecules, first in a canonical (*NVT*) ensemble for 100 ps, and then in an isothermal-isobaric (*NPT*) ensemble at 1 bar for another 100 ps. Then, 2 quartz surfaces were placed on the left and right sides of the box, with the Si-OH groups facing and interacting with the solution. Another energy minimization was performed, after which the system was finally sampled for 120 ns at 300 K in *NVT* ensemble with position restraints on all silicon atoms of the quartz surfaces.

Table 1. Details of the Simulated Systems

System	N_{quartz}	N_{VO-79}	$N_{toluene}$	$N_{n\text{-heptane}}$	Time (ns)
H100	2	24	0	1331	120
HT25	2	24	459	998	120
HT50	2	24	918	666	120
HT75	2	24	1376	333	120
T100	2	24	1835	0	120

2.2 Simulation Details. The GROMACS 5.0.4 simulation package[63, 64] was used to carry out the MD simulations with periodic boundary conditions applied in all three directions. Maxwell distribution was used to generate the initial velocities of atoms. LINCS algorithm was applied to constrain all bonds,[65] and a time step of 1 fs was used to integrate the equations of motion. Long-range electrostatic interactions were handled by Particle-mesh Ewald (PME) method,[66, 67] with a Fourier grid spacing of 0.16 nm. A twin-range cutoff scheme was used for short-range electrostatics and van der Waals interactions with a cutoff value of 1.4 nm. Temperature was controlled by applying the V-rescale thermostat[68] with coupling time (τ_T) set at 0.1 ps, and pressure in the *NPT* simulation was controlled using the Parrinello-Rahman barostat[69] with coupling time (τ_P)

set at 2.0 ps. Appropriate post-processing programs available in GROMACS were used for trajectory analysis and VMD[70] for visualization. Multiwfn 3.3.9 program[71] was employed to localize and identify the non-covalent interactions (NCI), which was introduced by Johnson *et al.*[72]

3. RESULTS AND DISCUSSION

3.1 Diffusion. Root mean square deviations (RMSD) of the VO-79 molecules in all systems are plotted as functions of time in Figure 2a, which clearly demonstrate the attainment of equilibrium in the end. For system H100, there is little change in RMSD after 40 ns, while it takes much longer for system T100 (about 90 ns) to reach equilibrium. The time to reach equilibrium for the remaining 3 systems is between these two cases. In addition, the equilibrium RMSD value is lower in *n*-heptane (H100) than that in the other four systems containing toluene. The results suggest that due to its poor solubility in *n*-heptane,[73, 74] the VO-79 molecules in system H100 experienced fastest adsorption onto the quartz surface, which quickly reduced their mobility.

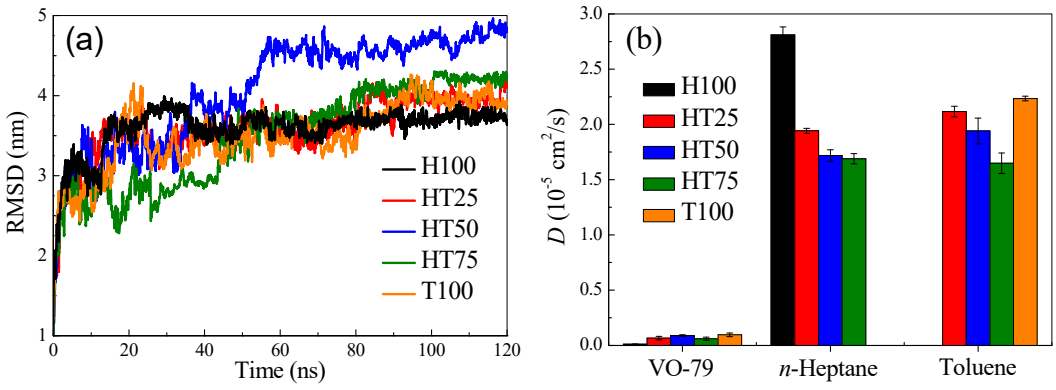

Figure 2. (*a*) Time evolution of root mean square deviation (RMSD) of VO-79 molecules, and (*b*) diffusion coefficients (*D*) of VO-79, *n*-heptane and toluene in the 5 simulated systems.

To quantify the mobility of the molecules in the simulated systems, the diffusion coefficient (*D*) was calculated from the slope of the mean square displacement (MSD) according to the Einstein relation:[75]

$$D = \frac{1}{6}\lim_{t\to\infty}\frac{d}{dt}\left\langle \left|\mathbf{r}(t)-\mathbf{r}(0)\right|^2 \right\rangle \qquad (1)$$

where $\mathbf{r}(t)$ and $\mathbf{r}(0)$ are the center of mass (COM) position of each individual molecule at time t and 0, respectively, and the average $\langle|\mathbf{r}(t)-\mathbf{r}(0)|^2\rangle$ is conducted over all molecules of the same type. The time-dependent MSD of individual components are given in Section S1 of Supporting Information (SI), and the corresponding diffusion coefficients are shown in Figure 2b. First consider the solvent molecules. The D value of *n*-heptane in H100 is found to be $(2.81 \pm 0.07) \times 10^{-5}$ cm^2/s, and that of toluene in T100 is $(2.23 \pm 0.02) \times 10^{-5}$ cm^2/s, both in good agreement with the published experimental values: 3.12×10^{-5} and 2.26×10^{-5} cm^2/s for bulk *n*-heptane[76-78] and toluene[79], respectively. In heptol (HT25, HT50, HT75), the diffusion coefficients of *n*-heptane and toluene are both smaller than their values in the pure solvent cases (H100, T100). The attractive interaction between *n*-heptane and toluene was found to be stronger than that between the same species (see Section S2 in SI), which could be the reason why diffusion is faster in the pure solvents. The D values in heptol also decrease with decreasing proportion of *n*-heptane, which is consistent with earlier studies[80, 81] in which the diffusion coefficients of binary mixtures decrease with decreasing alkane content.

While the diffusion of *n*-heptane and toluene can be reasonably well modeled by the Einstein relation, the diffusion of VO-79 is anomalous (non-Einstein),[82, 83] and the relation between MSD and time does not follow a straight line (Figure S1a). In these cases, to estimate the diffusion coefficients, we employed the method proposed in the literature,[36] namely, only the MD trajectories that can be approximated by Einstein diffusion were extracted for analysis. The calculated diffusion coefficients of VO-79 are also shown in Figure 2b. Compared with the solvents, the D values of VO-79 are significantly (1–2 orders of magnitude) smaller: it is $(0.10 \pm 0.02) \times 10^{-5}$ cm^2/s in T100 and $(0.01 \pm 0.01) \times 10^{-5}$ cm^2/s in H100. The much small D in H100 is consistent with the distinct solubility of asphaltene in toluene and *n*-heptane,[45, 84] being more soluble and dispersive in toluene. Furthermore, the D values of VO-79 in all systems are substantially lower than the previous experimental values ($0.24–0.35 \times 10^{-5}$ cm^2/s) measured for asphaltenes in bulk toluene solution.[85, 86] The reduced mobility suggests that VO-79 molecules may have experienced significant adsorption onto the quartz surface, which will be examined next.

3.2 Process and Mode of Adsorption. Representative snapshots taken at different time of the simulation trajectories are shown in Figure 3 to illustrate the adsorption process. The corresponding density distributions of individual components along the direction perpendicular to the quartz surfaces are shown in Section S3 of SI. As another validation of our results, the bulk density of *n*-heptane in H100 is found to be 676.6 kg/cm^3, and the bulk density of toluene in T100 is 860.5 kg/cm^3. These values agree very well with the published experimental values of 679.5 and 862.3 kg/cm^3 for pure *n*-heptane[87, 88] and toluene[88-90] respectively.

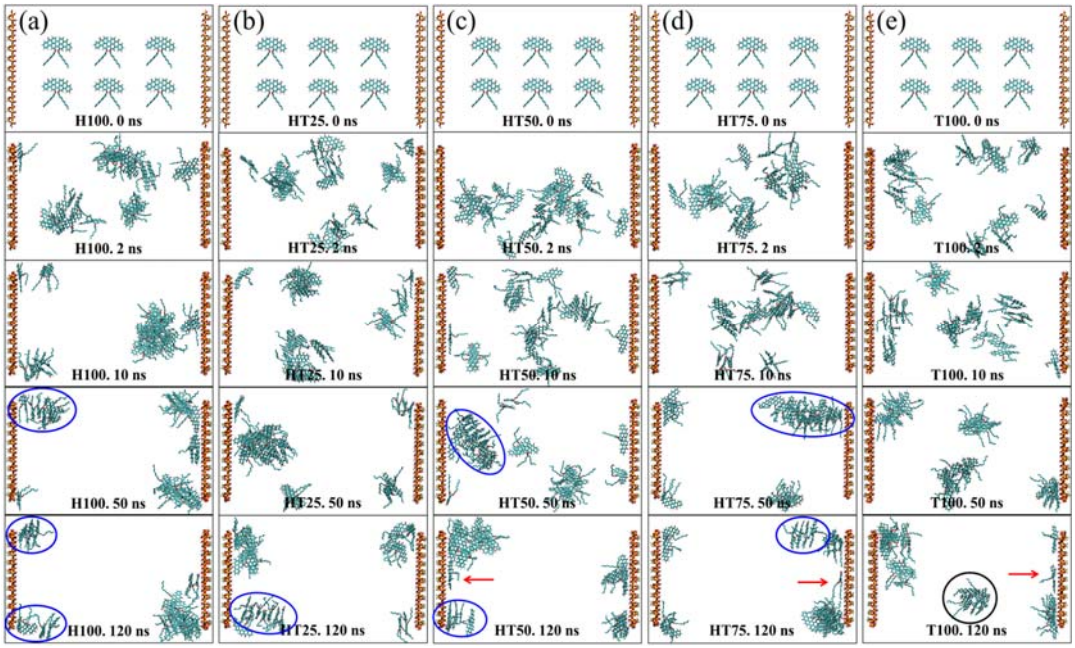

Figure 3. Representative snapshots of (*a*) H100, (*b*) HT25, (*c*) HT50, (*d*) HT75 and (*e*) T100 during the simulations. Each snapshot is labeled as X.m, representing the snapshot of the model system X (X = H100, HT25, HT50, HT75, T100) at the *m-th* ns. C, H, O and Si atoms are shown in cyan, white, red and yellow, respectively. Solvent molecules are not shown for clarity. Blue circles represent the one-dimensional (1D) rod-like structures formed by face-to-face π-π stacking of the PACs, while black circle represents the three-dimensional (3D) sphere-like structure. Red arrows point to the VO-79 molecules adsorbed on the surfaces in monomer form.

As seen in Figure 3a, within the first 2 ns some VO-79 molecules in *n*-heptane

already adsorbed on the quartz surface, as either monomer or dimer. Meanwhile the other VO-79 formed aggregates in the bulk solvent, and no VO-79 existed in the bulk in monomer form. Between 2 ns and 10 ns, these aggregates migrated from the bulk towards the quartz surface, and adhered to the monomers and dimers that adsorbed previously. Dynamic re-arrangement of the adsorbed molecules occurred afterwards near the two surfaces, without desorption of the molecules back into the bulk. In the late stage of the simulation (50 ns and 120 ns), all VO-79 molecules are stably adsorbed to the surface in the form of several large aggregates. Observations in heptol and toluene (Figure 3b–3e) are similar to that in *n*-heptane, but with a few differences. Firstly, the adsorption of VO-79 in these four systems is slower than in *n*-heptane. At 2 ns, only one monomer showed adsorption in systems HT25 and HT50, and adsorption did not start in system HT75 and T100. Secondly, at the end of the simulation, system T100 exhibited a different configuration than the other systems. In particular, a fraction of VO-79 molecules and their aggregates preferred to stay in the bulk phase rather than on the surfaces.

It is clear from above that the type of solvent has a great influence on the kinetics of adsorption. Visual examination of the simulation trajectories also revealed two modes of adsorption: in the forms of monomers or aggregates. To quantitative understand the process and mode of adsorption, the numbers of adsorbed VO-79 molecules are plotted in Figure 4a for different simulation time (see Section S4 in SI for details of the calculation). The numbers are further separated according to the two observed modes: monomers or aggregates. At the end of the simulations (120 ns), all 24 VO-79 molecules were adsorbed on the surfaces except in system T100. Move evident difference among the systems exists in the rate and mode of the adsorption.

In H100, the fastest adsorption occurs between 2 and 10 ns, during which the number of adsorbed molecules increases from 3 to 22. The maximum adsorption rate can be calculated to be (22 – 3) / (10 – 2 ns) = 2.4 ns^{-1}. All the 24 VO-79 molecules become adsorbed by 20 ns and they stay on the surface afterwards. So the average adsorption rate can be estimated to be 24 / (20 ns) = 1.2 ns^{-1}. In heptol, the fastest adsorption occurs between 50 and 60 ns regardless of the *n*-heptane/toluene ratio, and the maximum

adsorption rates for HT25, HT50 and HT75 are 1.5, 1.1 and 1.9 ns^{-1}, respectively. However, the time taken to complete the adsorption is different for the 3 systems, and the average adsorption rates are 0.20, 0.34 and 0.40 ns^{-1} for HT25, HT50 and HT75, respectively. In toluene, the fastest adsorption occurs between 30 and 40 ns, with the maximum adsorption rate of 0.6 ns^{-1}. Only 14 molecules are adsorbed on the surfaces after 120 ns, resulting in a low average adsorption rate of 0.12 ns^{-1}. The maximum and average adsorption rates are plotted in Figure 4b for all the systems, which exhibit a similar trend. When toluene is added into pure *n*-heptane solution, both adsorption rates decrease markedly, and then increase moderately with increasing proportion of toluene. Once the toluene content reaches 100%, both rates drop again, with significantly smaller values than those in *n*-heptane.

From Figure 4a, both monomer and aggregate adsorptions are observed in the five systems, the latter more dominant during the adsorption process. In *n*-heptane, all VO-79 molecules are adsorbed in the form of aggregates except one monomer at 2 ns. These aggregates are very stable after 10 ns, and there is no transition between the two adsorption modes. In HT25, the adsorption is entirely in the form of monomer for the first 10 ns. Then the number of adsorbed molecules increases considerably with the appearance of aggregate adsorption, with reversible transitions between the two modes. The scenario is similar in HT50, although monomer adsorption dominates for the first 40 ns. In contrast, in HT75, the adsorption starts with aggregates, and they are stable on the surfaces with only transition towards monomer adsorption in the final stage. Comparable to HT25 and HT50, adsorption in toluene also begins with monomers, followed by the adsorption of aggregates and reversible transitions between two modes throughout the process. However the overall adsorbed molecules are less, due to the molecules that remain solvated in bulk toluene.

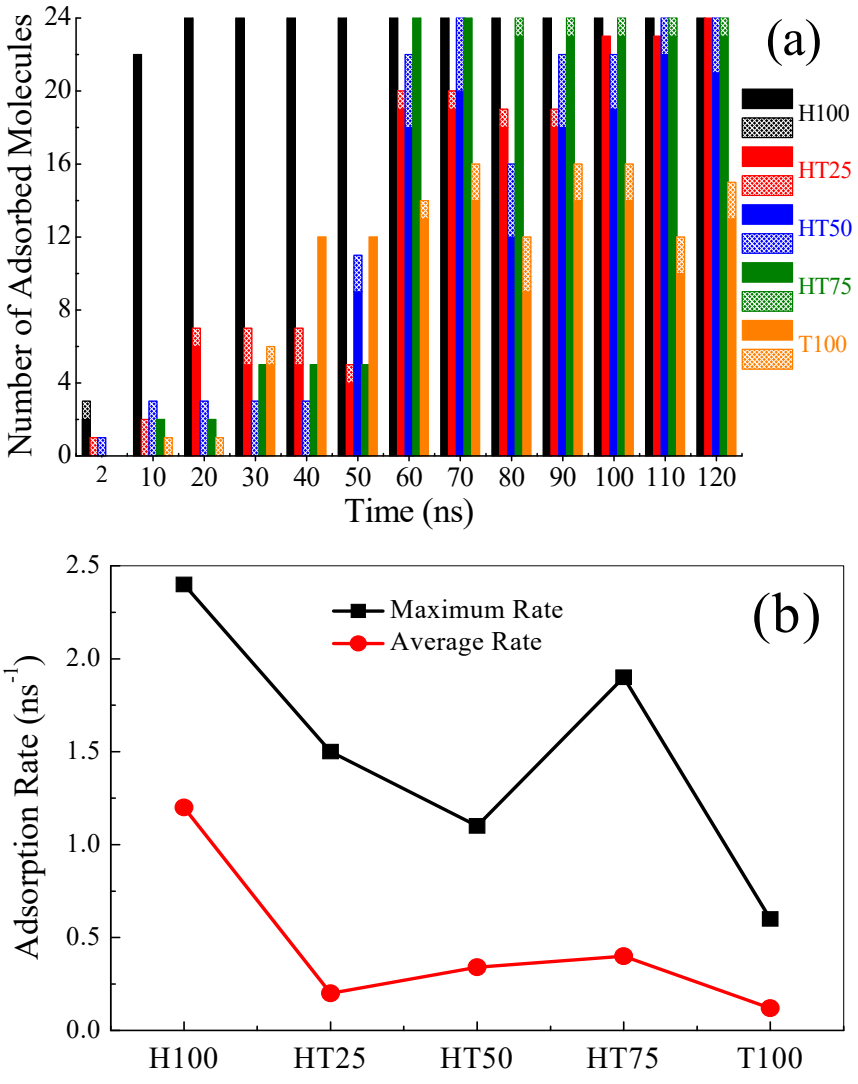

Figure 4. (*a*) Number of adsorbed VO-79 molecules at different simulation time. Solid columns correspond to number of molecules adsorbed in the form of aggregates while shaded columns correspond to number of molecules adsorbed in the form of monomers. (*b*) The maximum and average adsorption rates of VO-79 molecules in the 5 simulated systems.

The effective thickness of the adsorbed layers can be evaluated (see Section S3 for details of the calculation) and are shown in Table 2. Since there are two quartz surfaces (see Figure 3) in each system, the thicknesses on the left and right surfaces are reported separately, along with their sum (total thickness). The maximum thicknesses in system H100, HT25, HT50, HT75 and T100 are 4.05 nm, 4.31 nm, 4.55 nm, 5.03 nm and 3.83

nm, respectively. These values are close to the experimentally measured thickness of asphaltene layers (6.2–8.7 nm) adsorbed from xylene solution onto a hydrophilic silica surface.[22] It was also reported that after the addition of 30% heptane into the xylene solution, the thickness of the adsorbed asphaltene layer increased from 7.4 to 10.3 nm. This is in qualitative agreement with our results that as *n*-heptane is added to toluene (comparing the heptol systems with T100), the adsorbed layers become thicker. More interestingly, the thicknesses in the heptol systems are also larger than the value in *n*-heptane. At first glance, this is counter-intuitive, since the solubility of VO-79 in heptol should be between that in *n*-heptane and toluene. Careful examination of Figure 3 reveals an interesting structure formed by the VO-79 aggregates adsorbed on the quartz surface. Some aggregates exhibit the shape of a one-dimensional (1D) rod (indicated by blue circles in Figure 3) where the PACs of the molecules in the aggregate stack to each other face-to-face over a relatively long range. These 1D structures are more significant in the heptol systems and effectively increase the thickness of the adsorbed layer. Jian et al.[91] investigated the formation of such a 1D structure by VO-78 in bulk solvents (in absence of any solid surfaces), and found that the longest range of stacking was obtained by having a small amount of toluene in *n*-heptane. Similar phenomenon is also observed here for VO-79 adsorption on quartz. The presence of toluene in heptol allows the VO-79 molecules to have better solubility and mobility to rearrange themselves to form the 1D rod near the surfaces, thus increasing the thickness.

Table 2. Thickness of the Adsorbed VO-79 Layers (nm)

Systems	Left Layer	Right Layer	Total Thickness
H100	3.57	4.05	7.62
HT25	4.31	3.11	7.42
HT50	4.55	2.63	7.18
HT75	2.15	5.03	7.18
T100	3.83	2.15	5.97

The orientation of PAC plane of adsorbed VO-79 molecules relative to the quartz

surfaces was calculated by the cosine of angle θ ($\cos\theta$) between them. Figure 5 shows the fraction of molecules in different ranges of $\cos\theta$, data averaged over the last 10 ns of the simulations. θ can vary from 0° to 90°, thus $\cos\theta$ is in the range of 0 to 1. When $0 \leq \cos\theta \leq 0.2$, the PAC plane of a VO-79 can be considered to be almost perpendicular to the quartz surface. When $0.9 \leq \cos\theta \leq 1$, the molecule is considered being parallel to the surface. Between these two limits, the molecule is considered to be in the slant state. Sample images of these configurations can be found in Section S5 of SI. From Figure 5, it is clear that $\cos\theta$ of VO-79 with monomer adsorption (shaded columns) are distributed exclusively in the range of 0.9–1, indicating that if a VO-79 molecule is adsorbed as a monomer, it tends to be parallel to the quartz surface. Examination of the adsorption process of these monomers shows that they are first attached to the quartz surface with a nearly perpendicular configuration, but quickly transitions into a slant and then parallel configuration (see Section S6 of SI). In comparison, $\cos\theta$ of VO-79 adsorbed as aggregates (solid columns) has a wider distribution (0.1–1), with some molecules in a parallel configuration (0.9–1) but more taking a slant configuration (0.2–0.9). Very few molecules are in a perpendicular configuration (0–0.2).

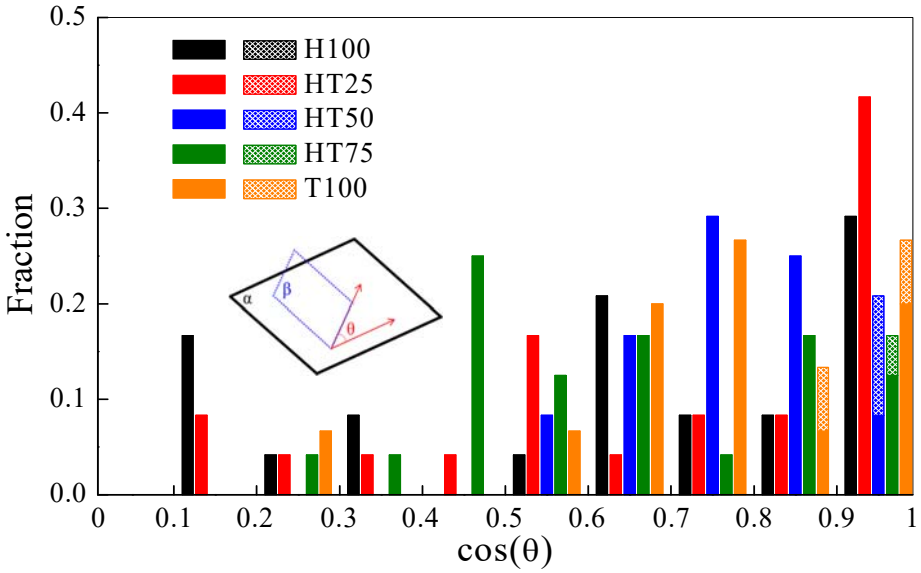

Figure 5. Distribution of cosine of angle θ ($\cos\theta$) between quartz surfaces and PAC plane of adsorbed VO-79 molecules, averaged over the last 10 ns of the simulations. Inset: schematic depiction of the calculation of $\cos\theta$ between planes α and β, which are

respectively the plane of the quartz surface and the PAC plane of the VO-79 molecule adsorbed on the surface. Solid columns correspond to molecules adsorbed in the form of aggregates while shaded columns correspond to molecules adsorbed in the form of monomers.

3.3 Adsorption Mechanism. To understand the mechanism of VO-79 adsorption on quartz surfaces and the effect of different solvents, the van der Waals (ΔE_{vdW}) and electrostatic (ΔE_{elec}) interaction energies between VO-79 and quartz surfaces are plotted in Figure 6, along with the change in free energy of solvation (ΔG_{solv}) (see Section S7 of SI) evaluated based on the solvent accessible surface area (SASA)[92]. The results clearly show that vdW interaction is the main driving force for adsorption, while electrostatics and free energy of solvation also make considerable contribution and the two interactions are comparable in magnitude. It should be pointed out that free energy of solvation has rarely been considered in the literature for similar systems, although it is a non-negligible contributor to the adsorption. As VO-79 become adsorbed and replace the solvent molecules near the quartz surface, the interaction energies between solvent and quartz increase (see Section S8 of SI). However, such increase is smaller in magnitude compared with the reduction in interaction energies between VO-79 and quartz, demonstrating that VO-79 adsorption on quartz is energetically favored compared with solvent adsorption.

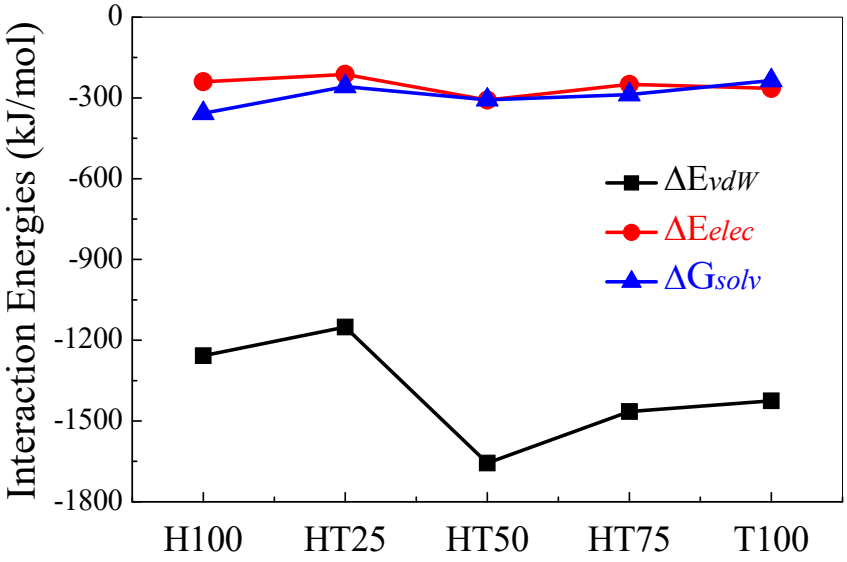

Figure 6. Interaction energies between quartz surfaces and VO-79 molecules in the 5 simulated systems.

To further identify the interaction characteristics between VO-79 molecules and quartz surfaces, non-covalent interaction (NCI) analysis[72, 93, 94] was carried out based on the electron density and reduced density gradient (RDG). The gradient isosurfaces resulting from the analysis are displayed in Figure 7 for an adsorbed aggregate in system HT50. The gradient isosurfaces are colored on a blue-green-red (BGR) scale according to the values of the electron density (ρ) multiplied by the sign of the second Hessian eigenvalue λ_2, i.e., sign(λ_2)ρ, which is a good indicator of the interaction strength. In general, large and negative values of sign(λ_2)ρ (blue) indicate strong attractive interactions (such as hydrogen bonds), while large and positive values (red) imply strong repulsive interactions (such as steric clashes). Values near zero (green) indicate weak interactions (such as van der Waals).[93, 94] It can be observed that the spaces between VO-79 and the quartz surface are mainly populated by color green, corresponding to van der Waals interactions between the aromatic rings of VO-79 and the silanol groups of quartz surface. Meanwhile, there are some blue dots, highlighted by black arrows in the inset, which suggests the presence of hydrogen bonding between VO-79 and the quartz surface. Similar results are found in other systems (Section S9 of SI), which indicated that in solvents with different solubility, the natures of NCI of

VO-79 with quartz surface are similar. In addition, the gradient isosurfaces appear to be green between VO-79 molecules, which correspond to the π-π interactions between the neighboring PACs. The importance of van der Waals interactions between VO-79 and quartz, and the π-π interactions between neighboring VO-79 molecules are consistent with previous experimental and theoretical studies.[20, 25, 36, 37]

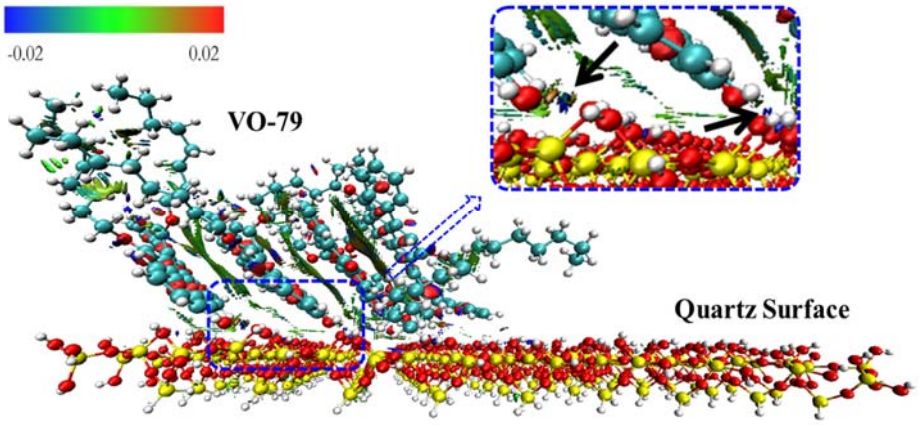

Figure 7. Gradient isosurfaces (s = 0.25 a.u.) for the interactions between a VO-79 aggregate and a quartz surface in system HT50. The surfaces are colored on a blue-green-red (BGR) scale according to the corresponding values of sign(λ_2)ρ, ranging from –0.02 to +0.02 a.u. Blue represents the strong attractive interactions, green weak interactions, and red strong repulsive interactions.

3.4 Discussion. As presented above, the adsorption modes of VO-79 molecules on quartz surfaces can be divided into two categories: monomer and aggregate adsorptions. VO-79 always adsorb on quartz surface as monomers or dimers in the initial stage, followed by the adsorption of aggregates pre-formed in bulk solvents. This observation is consistent with the previously reported asphaltenes adsorption on solid surfaces, which consisted of two steps: first monolayer adsorption, and then monolayer to multilayer transition[21, 22] leading to the formation of very large, slowly diffusing asphaltene aggregates, even in toluene.[11] Moreover, our work provides structural details regarding the adsorbed layers. Specifically, the PACs of VO-79 adsorbed as monomers are merely parallel to the surface, while the PACs in aggregate adsorption represent two

types of orientations: parallel and slant. Configurations in which the PACs are perpendicular to the surface are rare, that is, there is a tendency to enhance the interaction between VO-79 aggregates and the quartz surface by increasing the contact area between the directly adsorbed VO-79 and the surface.

In previous studies, the adsorption of asphaltenes on mica surface was identified as being controlled by the diffusion of asphaltenes from the bulk solution to the surface,[10] and the amount of asphaltene adsorption on hydrophilic silica particles increased with the increasing ratio of pentane to toluene.[11] Our simulations also show that the nature of solvent influences the kinetics of adsorption, such as the adsorption rate and final adsorption amount. Due to the different solubilities in *n*-heptane and toluene (*n*-heptane: "bad" solvent; toluene: "good" solvent), asphaltenes exhibit distinct geometries in the bulk solvents: 1D rod-like structures are dominant in *n*-heptane, while short-cylinder and sphere-like structures are formed in toluene.[95] Similar phenomena are also observed in this work for VO-79 adsorption on quartz. In particular, the formation of 1D rod-like structures has effectively increased the thickness of the adsorbed layers in *n*-heptane and heptol, even leading to thicker layers in heptol than in pure *n*-heptane.

Xiong et al. simulated the adsorption of C5Pe on silica in a previous work.[37] The most significant structural difference between C5Pe and VO-79 is the presence of polar terminal groups in the SCs of C5Pe. With the polar terminal groups, it is easier for C5Pe to form hydrogen bonds with the silanol groups on the surface. This is confirmed by the hydrogen bond calculations (Section S10 of SI). The number of hydrogen bonds is also more sensitive to the type of solvent in the case of C5Pe. Despite these differences, the orientations of adsorbed C5Pe molecules relative to the surface follow a similar distribution to Figure 5, indicating that the equilibrium adsorption configuration is insensitive to the terminal groups. On the other hand, the polarity change in the SCs does affect the adsorption process. As demonstrated in Section S6 of SI, without any polar terminal groups, monomer adsorption of VO-79 is initiated by point contact of its PAC with the surface, while the adsorption of C5Pe with polar terminal groups is initiated via the carboxylic acid group. Another difference observed in our work is that VO-79 molecules adsorbed in the form of aggregates are able to maintain π-π stacking

between their PACs, in some cases over a quite long range, which was not seen for C5Pe.

4. CONCLUSION

The adsorption of violanthrone-79 based model asphaltenes compound on quartz surface in different organic solvents was investigated by MD simulations. The type of solvent showed a great impact on the kinetics of adsorption, including the adsorption rate and final adsorption amount. However, the equilibrium modes of adsorption were similar: both monomer and aggregate adsorptions were observed in *n*-heptane, toluene and heptol. With monomer adsorption, the PAC of VO-79 was merely parallel to quartz surface, while the PACs in aggregate adsorption showed two types of orientations: parallel and slant, with the majority of them slant to the surface maintaining π-π stacking between neighboring PACs. Van der Waals interactions were found to contribute most to the adsorption, accompanied by electrostatics, hydrogen bonding and free energy of solvation.

■ ASSOCIATED CONTENT

Supporting Information

The Supporting Information is available free of charge on the ACS Publications website at DOI:

MSD, average interaction energy, mass density, definitions and configurations of monomer and aggregate adsorption, process of monomer adsorption, free energy of solvation, change of interaction energy, additional NCI analysis, calculation of hydrogen bonds (PDF)

■ AUTHOR INFORMATION

Corresponding Authors

*(H.Z.) Phone: +1-780-492-1044; E-mail: hongbo.zeng@ualberta.ca.

*(T.T.) Phone: +1-780-492-5467; E-mail: tian.tang@ualberta.ca.

ORCID

Tu Lan: 0000-0002-9877-2636

Tian Tang: 0000-0002-2387-3571

Hongbo Zeng: 0000-0002-1432-5979

Notes

The authors declare no competing financial interest.

■ ACKNOWLEDGMENTS

We acknowledge the computing resources and technical support from Western Canada Research Grid (WestGrid). Financial support from the Natural Science and Engineering Research Council (NSERC) of Canada, and the Future Energy Systems under the Canada First Research Excellence Fund and the Canada Research Chairs Program is gratefully acknowledged. We would also like to thank Dr. Alpesh K. Malde, School of Chemistry and Molecular Biosciences, University of Queensland, Australia, and Xiaoyu Sun, Department of Chemical and Materials Engineering, University of Alberta, Canada, for generously providing the force field parameters for quartz and VO-79, respectively.

■ REFERENCES

(1) Adams, J. J. Asphaltene adsorption, a literature review. *Energy Fuels* **2014,** *28*, 2831-2856.

(2) Jiang, T.; Hirasaki, G. J.; Miller, C. A.; Ng, S. Wettability alteration of clay in solid-stabilized emulsions. *Energy Fuels* **2011,** *25*, 2551-2558.

(3) Jada, A.; Debih, H. Hydrophobation of clay particles by asphaltenes adsorption. *Compos. Interfaces* **2009,** *16*, 219-235.

(4) Jada, A.; Debih, H.; Khodja, M. Montmorillonite surface properties modifications by asphaltenes adsorption. *J. Petrol. Sci. Eng.* **2006,** *52*, 305-316.

(5) Kumar, K.; Dao, E.; Mohanty, K. AFM study of mineral wettability with reservoir oils. *J. Colloid Interface Sci.* **2005,** *289*, 206-217.

(6) Cosultchi, A.; Cordova, I.; Valenzuela, M. A.; Acosta, D. R.; Bosch, P.; Lara, V. H. Adsorption of crude oil on Na^{+}-Montmorillonite. *Energy Fuels* **2005,** *19*, 1417-1424.

(7) Pernyeszi, T.; Patzko, A.; Berkesi, O.; Dékány, I. Asphaltene adsorption on clays and crude oil reservoir rocks. *Colloids Surf., A* **1998,** *137*, 373-384.

(8) Liu, J.; Wang, J.; Huang, J.; Cui, X.; Tan, X.; Liu, Q.; Zeng, H. Heterogeneous distribution of adsorbed bitumen on fine solids from solvent-based extraction of oil sands probed by AFM. *Energy Fuels* **2017,** *31*, 8833-8842.

(9) Gonzalez, V.; Taylor, S. E. Asphaltene adsorption on quartz sand in the presence of pre-adsorbed water. *J. Colloid Interface Sci.* **2016,** *480*, 137-145.

(10) Natarajan, A.; Kuznicki, N.; Harbottle, D.; Masliyah, J.; Zeng, H.; Xu, Z. Understanding mechanisms of asphaltene adsorption from organic solvent on mica. *Langmuir* **2014,** *30*, 9370-9377.

(11) Zahabi, A.; Gray, M. R.; Dabros, T. Kinetics and properties of asphaltene adsorption on surfaces. *Energy Fuels* **2012,** *26*, 1009-1018.

(12) Farooq, U.; Sjøblom, J.; Øye, G. Desorption of asphaltenes from silica-coated quartz crystal

surfaces in low saline aqueous solutions. *J. Dispers. Sci. Technol.* **2011,** *32*, 1388-1395.

(13) Pernyeszi, T.; Dékány, I. Sorption and elution of asphaltenes from porous silica surfaces. *Colloids Surf., A* **2001,** *194*, 25-39.

(14) Lopez-Linares, F.; Carbognani, L.; Hassan, A.; Pereira-Almao, P.; Rogel, E.; Ovalles, C.; Pradhan, A.; Zintsmaster, J. Adsorption of Athabasca vacuum residues and their visbroken products over macroporous solids: Influence of their molecular characteristics. *Energy Fuels* **2011,** *25*, 4049-4054.

(15) Xing, C.; Hilts, R.; Shaw, J. Sorption of Athabasca vacuum residue constituents on synthetic mineral and process equipment surfaces from mixtures with pentane. *Energy Fuels* **2010,** *24*, 2500-2513.

(16) Saraji, S.; Goual, L.; Piri, M. Adsorption of asphaltenes in porous media under flow conditions. *Energy Fuels* **2010,** *24*, 6009-6017.

(17) González, M. F.; Stull, C. S.; López-Linares, F.; Pereira-Almao, P. Comparing asphaltene adsorption with model heavy molecules over macroporous solid surfaces. *Energy Fuels* **2007,** *21*, 234-241.

(18) Tu, Y.; Kingston, D.; Kung, J.; Kotlyar, L. S.; Sparks, B. D.; Chung, K. H. Adsorption of pentane insoluble organic matter from oilsands bitumen onto clay surfaces. *Pet. Sci. Technol.* **2006,** *24*, 327-338.

(19) Wang, S.; Liu, Q.; Tan, X.; Xu, C.; Gray, M. R. Study of asphaltene adsorption on kaolinite by X-ray photoelectron spectroscopy and time-of-flight secondary ion mass spectroscopy. *Energy Fuels* **2013,** *27*, 2465-2473.

(20) Liu, X.; Yan, W.; Stenby, E. H.; Thormann, E. Release of crude oil from silica and calcium carbonate surfaces: On the alternation of surface and molecular forces by high- and low-salinity aqueous salt solutions. *Energy Fuels* **2016,** *30*, 3986-3993.

(21) de la Cruz, J. L. M.; Castellanos-Ramírez, I. V.; Ortiz-Tapia, A.; Buenrostro-González, E.; Durán-Valencia, C. d. l. A.; López-Ramírez, S. Study of monolayer to multilayer adsorption of asphaltenes on reservoir rock minerals. *Colloids Surf., A* **2009,** *340*, 149-154.

(22) Jouault, N.; Corvis, Y.; Cousin, F.; Jestin, J.; Barré, L. Asphaltene adsorption mechanisms on the local scale probed by neutron reflectivity: Transition from monolayer to multilayer growth above the flocculation threshold. *Langmuir* **2009,** *25*, 3991-3998.

(23) Dudášová, D.; Simon, S.; Hemmingsen, P. V.; Sjöblom, J. Study of asphaltenes adsorption onto different minerals and clays: Part 1. Experimental adsorption with UV depletion detection. *Colloids Surf., A* **2008,** *317*, 1-9.

(24) Zhang, L.; Shi, C.; Lu, Q.; Liu, Q.; Zeng, H. Probing molecular interactions of asphaltenes in heptol using a surface forces apparatus: Implications on stability of water-in-oil emulsions. *Langmuir* **2016,** *32*, 4886-95.

(25) Murgich, J. Intermolecular forces in aggregates of asphaltenes and resins. *Pet. Sci. Technol.* **2002,** *20*, 983-997.

(26) Jian, C.; Tang, T.; Bhattacharjee, S. Probing the effect of side-chain length on the aggregation of a model asphaltene using molecular dynamics simulations. *Energy Fuels* **2013,** *27*, 2057-2067.

(27) Mikami, Y.; Liang, Y.; Matsuoka, T.; Boek, E. S. Molecular dynamics simulations of asphaltenes at the oil–water interface: From nanoaggregation to thin-film formation. *Energy Fuels* **2013,** *27*, 1838-1845.

(28) Jian, C.; Tang, T.; Bhattacharjee, S. Molecular dynamics investigation on the aggregation of violanthrone78-based model asphaltenes in toluene. *Energy Fuels* **2014,** *28*, 3604-3613.

(29) Jian, C.; Tang, T. Molecular dynamics simulations reveal inhomogeneity-enhanced stacking of violanthrone-78-based polyaromatic compounds in *n*-heptane-toluene mixtures. *J. Phys. Chem. B* **2015,** *119*, 8660-8668.

(30) Liu, J.; Zhao, Y.; Ren, S. Molecular dynamics simulation of self-aggregation of asphaltenes at an oil/water interface: Formation and destruction of the asphaltene protective film. *Energy Fuels* **2015,** *29*, 1233-1242.

(31) Jian, C.; Zeng, H.; Liu, Q.; Tang, T. Probing the adsorption of polycyclic aromatic compounds onto water droplets using molecular dynamics simulations. *J. Phys. Chem. C* **2016,** *120*, 14170-14179.

(32) Kuznicki, T.; Masliyah, J. H.; Bhattacharjee, S. Aggregation and partitioning of model asphaltenes at toluene−water interfaces: Molecular dynamics simulations. *Energy Fuels* **2009,** *23*, 5027-5035.

(33) Teklebrhan, R. B.; Ge, L.; Bhattacharjee, S.; Xu, Z.; Sjöblom, J. Initial partition and aggregation of uncharged polyaromatic molecules at the oil–water interface: A molecular dynamics simulation study. *J. Phys. Chem. B* **2014,** *118*, 1040-1051.

(34) Gao, F.; Xu, Z.; Liu, G.; Yuan, S. Molecular dynamics simulation: The behavior of asphaltene in crude oil and at the oil/water interface. *Energy Fuels* **2014,** *28*, 7368-7376.

(35) Jian, C.; Liu, Q.; Zeng, H.; Tang, T. Effect of model polycyclic aromatic compounds on the coalescence of water-in-oil emulsion droplets. *J. Phys. Chem. C* **2017,** *121*, 10382-10391.

(36) Wu, G.; He, L.; Chen, D. Sorption and distribution of asphaltene, resin, aromatic and saturate fractions of heavy crude oil on quartz surface: Molecular dynamic simulation. *Chemosphere* **2013,** *92*, 1465-1471.

(37) Xiong, Y.; Cao, T.; Chen, Q.; Li, Z.; Yang, Y.; Xu, S.; Yuan, S.; Sjöblom, J.; Xu, Z. Adsorption of a polyaromatic compound on silica surfaces from organic solvents studied by molecular dynamics simulation and AFM imaging. *J. Phys. Chem. C* **2017,** *121*, 5020-5028.

(38) Xiong, Y.; Li, Z.; Cao, T.; Xu, S.; Yuan, S.; Sjöblom, J.; Xu, Z. Synergistic adsorption of polyaromatic compounds on silica surfaces studied by molecular dynamics simulation. *J. Phys. Chem. C* **2018,** *122*, 4290-4299.

(39) Cyran, J. D.; Krummel, A. T. Probing structural features of self-assembled violanthrone-79 using two dimensional infrared spectroscopy. *J. Chem. Phys.* **2015,** *142*, 212435.

(40) Hmoudah, M.; Nassar, N. N.; Vitale, G.; El-Qanni, A. Effect of nanosized and surface-structural-modified nano-pyroxene on adsorption of violanthrone-79. *RSC Adv.* **2016,** *6*, 64482-64493.

(41) Zi, M.; Chen, D.; Ji, H.; Wu, G. Effects of asphaltenes on the formation and decomposition of methane hydrate: A molecular dynamics study. *Energy Fuels* **2016,** *30*, 5643-5650.

(42) Wang, J.; van der Tuuk Opedal, N.; Lu, Q.; Xu, Z.; Zeng, H.; Sjöblom, J. Probing molecular interactions of an asphaltene model compound in organic solvents using a surface forces apparatus (SFA). *Energy Fuels* **2011,** *26*, 2591-2599.

(43) Wang, J.; Lu, Q.; Harbottle, D.; Sjoblom, J.; Xu, Z.; Zeng, H. Molecular interactions of a polyaromatic surfactant C5Pe in aqueous solutions studied by a surface forces apparatus. *J. Phys. Chem. B* **2012,** *116*, 11187-96.

(44) Schuler, B.; Meyer, G.; Peña, D.; Mullins, O. C.; Gross, L. Unraveling the molecular structures of asphaltenes by atomic force microscopy. *J. Am. Chem. Soc.* **2015,** *137*, 9870-9876.

(45) Teklebrhan, R. B.; Ge, L.; Bhattacharjee, S.; Xu, Z.; Sjöblom, J. Probing structure–nanoaggregation relations of polyaromatic surfactants: A molecular dynamics simulation and dynamic light scattering study. *J. Phys. Chem. B* **2012,** *116*, 5907-5918.

(46) Sodero, A. C. R.; Silva, H. S.; Level, P. G.; Bouyssiere, B.; Korb, J.-P.; Carrier, H.; Alfarra, A.; Bégué, D.; Baraille, I. Investigation of the effect of sulfur heteroatom on asphaltene aggregation. *Energy Fuels* **2016,** *30*, 4758-4766.

(47) Silva, H. S.; Sodero, A. C. R.; Bouyssiere, B.; Carrier, H.; Korb, J.-P.; Alfarra, A.; Vallverdu, G.; Bégué, D.; Baraille, I. Molecular dynamics study of nanoaggregation in asphaltene mixtures: Effects of the N, O, and S heteroatoms. *Energy Fuels* **2016,** *30*, 5656-5664.

(48) Li, Y.; Han, S.; Lu, Y.; Zhang, J. Influence of asphaltene polarity on crystallization and gelation of waxy oils. *Energy Fuels* **2018,** *32*, 1491-1497.

(49) Wattana, P.; Fogler, H. S.; Yen, A.; Garcìa, M. D. C.; Carbognani, L. Characterization of polarity-based asphaltene subfractions. *Energy Fuels* **2005,** *19*, 101-110.

(50) Nalwaya, V.; Tantayakom, V.; Piumsomboon, P.; Fogler, S. Studies on asphaltenes through analysis of polar fractions. *Ind. Eng. Chem. Res.* **1999,** *38*, 964-972.

(51) Hair, M. L.; Hertl, W. Adsorption on hydroxylated silica surfaces. *J. Phys. Chem.* **1969,** *73*, 4269-4276.

(52) Parida, S. K.; Dash, S.; Patel, S.; Mishra, B. K. Adsorption of organic molecules on silica surface. *Adv. Colloid Interface Sci.* **2006,** *121*, 77-110.

(53) Rimola, A.; Costa, D.; Sodupe, M.; Lambert, J.-F.; Ugliengo, P. Silica surface features and their role in the adsorption of biomolecules: Computational modeling and experiments. *Chem. Rev.* **2013,** *113*, 4216-4313.

(54) Lorenz, C. D.; Webb, E. B.; Stevens, M. J.; Chandross, M.; Grest, G. S. Frictional dynamics of perfluorinated self-assembled monolayers on amorphous SiO_2. *Tribol. Lett.* **2005,** *19*, 93-98.

(55) Lee, S. H.; Rossky, P. J. A comparison of the structure and dynamics of liquid water at hydrophobic and hydrophilic surfaces—a molecular dynamics simulation study. *J. Chem. Phys.* **1994,** *100*, 3334-3345.

(56) Wensink, E. J. W.; Hoffmann, A. C.; Apol, M. E. F.; Berendsen, H. J. C. Properties of adsorbed water layers and the effect of adsorbed layers on interparticle forces by liquid bridging. *Langmuir* **2000,** *16*, 7392-7400.

(57) Yan, H.; Yuan, S. Molecular dynamics simulation of the oil detachment process within silica nanopores. *J. Phys. Chem. C* **2016,** *120*, 2667-2674.

(58) Zhang, P.; Xu, Z.; Liu, Q.; Yuan, S. Mechanism of oil detachment from hybrid hydrophobic and hydrophilic surface in aqueous solution. *J. Chem. Phys.* **2014,** *140*, 164702.

(59) Liu, Q.; Yuan, S.; Yan, H.; Zhao, X. Mechanism of oil detachment from a silica surface in aqueous surfactant solutions: Molecular dynamics simulations. *J. Phys. Chem. B* **2012,** *116*, 2867-2875.

(60) Jian, C.; Poopari, M. R.; Liu, Q.; Zerpa, N.; Zeng, H.; Tang, T. Mechanistic understanding of the effect of temperature and salinity on the water/toluene interfacial tension. *Energy Fuels* **2016,** *30*, 10228-10235.

(61) Jian, C.; Poopari, M. R.; Liu, Q.; Zerpa, N.; Zeng, H.; Tang, T. Reduction of water/oil interfacial tension by model asphaltenes: The governing role of surface concentration. *J. Phys. Chem. B* **2016,** *120*, 5646-5654.

(62) Jian, C.; Liu, Q.; Zeng, H.; Tang, T. A molecular dynamics study of the effect of asphaltenes on toluene/water interfacial tension: Surfactant or solute? *Energy Fuels* **2018,** *32*, 3225-3231.

(63) Hess, B.; Kutzner, C.; Van Der Spoel, D.; Lindahl, E. GROMACS 4: Algorithms for highly efficient, load-balanced, and scalable molecular simulation. *J. Chem. Theory Comput.* **2008,** *4*, 435-447.

(64) Pronk, S.; Páll, S.; Schulz, R.; Larsson, P.; Bjelkmar, P.; Apostolov, R.; Shirts, M. R.; Smith, J. C.; Kasson, P. M.; van der Spoel, D., et al. GROMACS 4.5: A high-throughput and highly parallel open source molecular simulation toolkit. *Bioinformatics* **2013,** *29*, 845-854.

(65) Hess, B. P-LINCS: A parallel linear constraint solver for molecular simulation. *J. Chem. Theory Comput.* **2008,** *4*, 116-122.

(66) Darden, T.; York, D.; Pedersen, L. Particle mesh Ewald: An N·log (N) method for Ewald sums in large systems. *J. Chem. Phys.* **1993,** *98*, 10089-10092.

(67) Essmann, U.; Perera, L.; Berkowitz, M. L.; Darden, T.; Lee, H.; Pedersen, L. G. A smooth particle mesh Ewald method. *J. Chem. Phys.* **1995,** *103*, 8577-8593.

(68) Bussi, G.; Donadio, D.; Parrinello, M. Canonical sampling through velocity rescaling. *J. Chem. Phys.* **2007,** *126*, 014101.

(69) Parrinello, M.; Rahman, A. Polymorphic transitions in single crystals: A new molecular dynamics method. *J. Appl. Phys.* **1981,** *52*, 7182-7190.

(70) Humphrey, W.; Dalke, A.; Schulten, K. VMD: Visual molecular dynamics. *J. Mol. Graph.* **1996,** *14*, 33-38.

(71) Lu, T.; Chen, F. Multiwfn: A multifunctional wavefunction analyzer. *J. Comput. Chem.* **2012,** *33*, 580-592.

(72) Johnson, E. R.; Keinan, S.; Mori-Sanchez, P.; Contreras-Garcia, J.; Cohen, A. J.; Yang, W. Revealing noncovalent interactions. *J. Am. Chem. Soc.* **2010,** *132*, 6498-6506.

(73) Speight, J. G.; Long, R. B.; Trowbridge, T. D. Factors influencing the separation of asphaltenes from heavy petroleum feedstocks. *Fuel* **1984,** *63*, 616-620.

(74) Yarranton, H. W.; Alboudwarej, H.; Jakher, R. Investigation of asphaltene association with vapor pressure osmometry and interfacial tension measurements. *Ind. Eng. Chem. Res.* **2000,** *39*, 2916-2924.

(75) Einstein, A. On the movement of small particles suspended in stationary liquids required by the molecular-kinetic theory of heat. *Ann. Phys.* **1905,** *17*, 549-560.

(76) Douglass, D. C.; McCall, D. W. Diffusion in paraffin hydrocarbons. *J. Phys. Chem.* **1958,** *62*, 1102-1107.

(77) McCall, D. W.; Douglass, D. C.; Anderson, E. W. Diffusion in liquids. *J. Chem. Phys.* **1959,** *31*, 1555-1557.

(78) Moore, J. W.; Wellek, R. M. Diffusion coefficients of *n*-heptane and *n*-decane in *n*-alkanes and *n*-alcohols at several temperatures. *J. Chem. Eng. Data* **1974,** *19*, 136-140.

(79) Antalek, B.; Williams, A. J.; Texter, J. Self-diffusion near the percolation threshold in reverse microemulsions. *Phys. Rev. E* **1996,** *54*, 5913-5916.

(80) Safi, A.; Nicolas, C.; Neau, E.; Chevalier, J.-L. Diffusion coefficients of aromatic compounds at infinite dilution in binary mixtures at 298.15 K. *J. Chem. Eng. Data* **2007,** *52*, 126-130.

(81) Pandey, J. D.; Mishra, R. K. Theoretical evaluation of thermal conductivity and diffusion coefficient of binary liquid mixtures. *Phys. Chem. Liq.* **2005,** *43*, 49-57.

(82) Baumgärtner, A.; Moon, M. Anomalous polymer diffusion between long rods. *Europhys. Lett.* **1989,** *9*, 203.

(83) Müller-Plathe, F.; Rogers, S. C.; van Gunsteren, W. F. Computational evidence for anomalous diffusion of small molecules in amorphous polymers. *Chem. Phys. Lett.* **1992,** *199*, 237-243.

(84) Yudin, I. K.; Nikolaenko, G. L.; Gorodetskii, E. E.; Markhashov, E. L.; Frot, D.; Briolant, Y.; Agayan, V. A.; Anisimov, M. A. Universal behavior of asphaltene aggregation in hydrocarbon solutions. *Pet. Sci. Technol.* **1998,** *16*, 395-414.

(85) Östlund, J.-A.; Nydén, M.; Auflem, I. H.; Sjöblom, J. Interactions between asphaltenes and naphthenic acids. *Energy Fuels* **2003,** *17*, 113-119.

(86) Andrews, A. B.; Guerra, R. E.; Mullins, O. C.; Sen, P. N. Diffusivity of asphaltene molecules by fluorescence correlation spectroscopy. *J. Phys. Chem. A* **2006,** *110*, 8093-8097.

(87) Aminabhavi, T.; Patil, V.; Aralaguppi, M.; Phayde, H. Density, viscosity, and refractive index of the binary mixtures of cyclohexane with hexane, heptane, octane, nonane, and decane at (298.15, 303.15,

and 308.15) K. *J. Chem. Eng. Data* **1996,** *41*, 521-525.

(88) Muringer, M.; Trappeniers, N.; Biswas, S. The effect of pressure on the sound velocity and density of toluene and *n*-heptane up to 2600 bar. *Phys. Chem. Liq.* **1985,** *14*, 273-296.

(89) Kashiwagi, H.; Hashimoto, T.; Tanaka, Y.; Kubota, H.; Makita, T. Thermal conductivity and density of toluene in the temperature range 273–373 K at pressures up to 250 MPa. *Int. J. Thermophys.* **1982,** *3*, 201-215.

(90) Assael, M.; Avelino, H.; Dalaouti, N.; Fareleira, J.; Harris, K. Reference correlation for the viscosity of liquid toluene from 213 to 373 K at pressures to 250 MPa. *Int. J. Thermophys.* **2001,** *22*, 789-799.

(91) Jian, C.; Tang, T. One-dimensional self-assembly of polyaromatic compounds revealed by molecular dynamics simulations. *J. Phys. Chem. B* **2014,** *118*, 12772-12780.

(92) Eisenhaber, F.; Lijnzaad, P.; Argos, P.; Sander, C.; Scharf, M. The double cubic lattice method: Efficient approaches to numerical integration of surface area and volume and to dot surface contouring of molecular assemblies. *J. Comput. Chem.* **1995,** *16*, 273-284.

(93) Contreras-García, J.; Yang, W.; Johnson, E. R. Analysis of hydrogen-bond interaction potentials from the electron density: Integration of noncovalent interaction regions. *J. Phys. Chem. A* **2011,** *115*, 12983-12990.

(94) Wu, P.; Chaudret, R.; Hu, X.; Yang, W. Noncovalent interaction analysis in fluctuating environments. *J. Chem. Theory Comput.* **2013,** *9*, 2226-2234.

(95) Jian, C.; Tang, T.; Bhattacharjee, S. A dimension map for molecular aggregates. *J. Mol. Graph. Model.* **2015,** *58*, 10-15.

TOC Graphic:

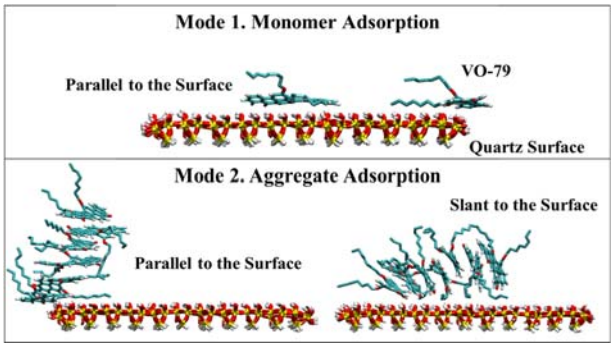
Mode 1. Monomer Adsorption
Parallel to the Surface
VO-79
Quartz Surface
Mode 2. Aggregate Adsorption
Slant to the Surface
Parallel to the Surface